High-Frequency Electromechanical Imaging of Ferroelectrics in a Liquid Environment

Nina Balke,[†,*] Stephen Jesse,[†] Ying-Hao Chu,[‡] and Sergei V. Kalinin[†]

[†]Center for Nanophase Materials Sciences, Oak Ridge National Laboratory, Oak Ridge, Tennessee 37831, United States and [‡]Department of Materials Science and Engineering, National Chiao Tung University, Hsinchu 30010, Taiwan

ABSTRACT The coupling between electrical and mechanical phenomena is a ubiquitous feature of many information and energy storage materials and devices. In addition to involvement in performance and degradation mechanisms, electromechanical effects underpin a broad spectrum of nanoscale imaging and spectroscopies including piezoresponse force and electrochemical strain microscopies. Traditionally, these studies are conducted under ambient conditions. However, applications related to imaging energy storage and electrophysiological phenomena require operation in a liquid phase and therefore the development of electromechanical probing techniques suitable to liquid environments. Due to the relative high conductivity of most liquids and liquid decomposition at low voltages, the transfer of characterization techniques from ambient to liquid is not straightforward. Here we present a detailed study of ferroelectric domain imaging and manipulation in thin film $BiFeO_3$ using piezoresponse force microscopy in liquid environments as model systems for electromechanical phenomena in general. We explore the use of contact resonance enhancement and the application of multifrequency excitation and detection principles to overcome the experimental problems introduced by a liquid environment. Understanding electromechanical sample characterization in liquid is a key aspect not only for ferroelectric oxides but also for biological and electrochemical sample systems.

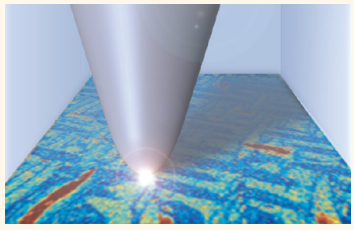

KEYWORDS: scanning probe microscopy · liquid · ferroelectrics

Electromechanical phenomena are universal features of a broad set of materials ranging from ferro- and piezoelectrics[1,2] to ionic systems such as batteries,[3] fuel cells,[4] and supercapacitors[5] and macromolecular[6,7] and biological[8] systems. In general, electromechanical effects are defined as a change in strain or stress as a result of an electrical stimulus. This can strongly affect the materials functionality or lifetime but can also be used as a basis for high-resolution imaging. The most prominent example are ferroelectric materials, broadly used for applications such as ferroelectric random access memories (FeRAM)[9] or microelectromechanical systems (MEMS).[10] Here, the electromechanical response of the sample to a varying ac field due to the piezoelectric effect can be used to detect domain orientations and local piezoelectric coefficients. This technique is referred to as piezoresponse force microscopy (PFM).[11−19] PFM can also be used to investigate biological systems, such as calcified tissue[20] and proteins.[21] Another example of systems with strong electromechanical coupling is Li-ion batteries. Here, the volume change is induced by a bias-driven change in ionic concentration in the material and the strong coupling between ionic concentration and molar volume.[22] The indirect detection of ion flows through strain has been utilized in electrochemical strain microscopy (ESM).[23,24]

In general, PFM and ESM experiments are performed under ambient conditions (*i.e.*, in air). However, for biological systems and many energy storage systems, submersion in liquid is desirable in order to provide a natural environment to stabilize biological samples and to investigate ionic transport across the electrolyte/electrode interface in energy storage materials. Recently, interfacial functionality of ferroelectric thin films in liquid environments was discussed in the context of (bio)molecular sensing and photoelectric applications.[25] These applications necessitate the development of PFM and ESM in conductive liquid environments. The main obstacles for this development are the difficulties related to applying electrical fields to the SPM tip in the presence of a conductive medium. Correspondingly, the efforts put toward accomplishing PFM in liquid has been extremely limited, including work by Rodriguez[26−28] that introduced the concept of high-frequency imaging and by Noh *et al.* working with shielded tips.[29] In both cases, imaging was performed by a single-frequency PFM, known to be highly

* Address correspondence to balken@ornl.gov.

Received for review April 4, 2012 and accepted May 9, 2012.

Published online May 09, 2012
10.1021/nn301489g

susceptible to topographic artifacts at high operational frequencies. At the same time, low-frequency excitation results in water splitting and spontaneous bubble formation when oxygen and hydrogen gases are formed.

Since then, several key advances in electromechanical imaging have been made, including the utilization of contact resonances through dual ac resonance tracking (DART)[30] and the band excitation (BE)[31] technique. These developments allow for higher sensitivities and measurement at higher frequencies, specifically obviating the indirect topographic cross-talk induced by variation in contact resonances.[32,33] Notably, AFM cantilever dynamics in liquids typically have very complicated transfer functions with multiple resonances ("forest of peaks") resulting in significant cross-talk.[34] Correspondingly, the use of DART and BE enable the use of high-frequency excitation, thus facilitating cross-talk free imaging in conductive environments without the need for shielded tips.

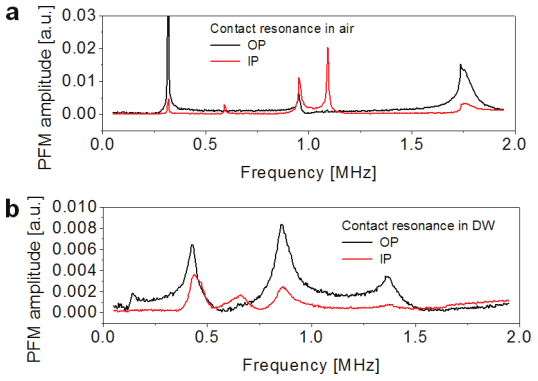

Figure 1. PFM amplitude as function of frequency of applied 1 V_{ac} voltage. Shown are OP and IP PFM component in (a) air and (b) DW.

Here, we explore the use of advanced techniques for electromechanical characterization in liquid environments, focusing on the elucidation of flexural and torsional cantilever contact dynamics. The change in contact dynamics going from air to liquid has been addressed theoretically[35] but not yet experimentally. The goal is to establish the opportunities and limitations of electromechanical characterization in liquid for ac and dc electrical fields which can be universally applied to PFM and ESM techniques.

RESULTS AND DISCUSSION

In this work, we focus on well-characterized ferroelectric thin films with strong electromechanical responses with different out-of-plane (OP) and in-plane (IP) polarization components. The experiments were performed on (001)-oriented multiferroic $BiFeO_3$ (BFO) thin films,[36] and single[37] and multiple[31] frequency

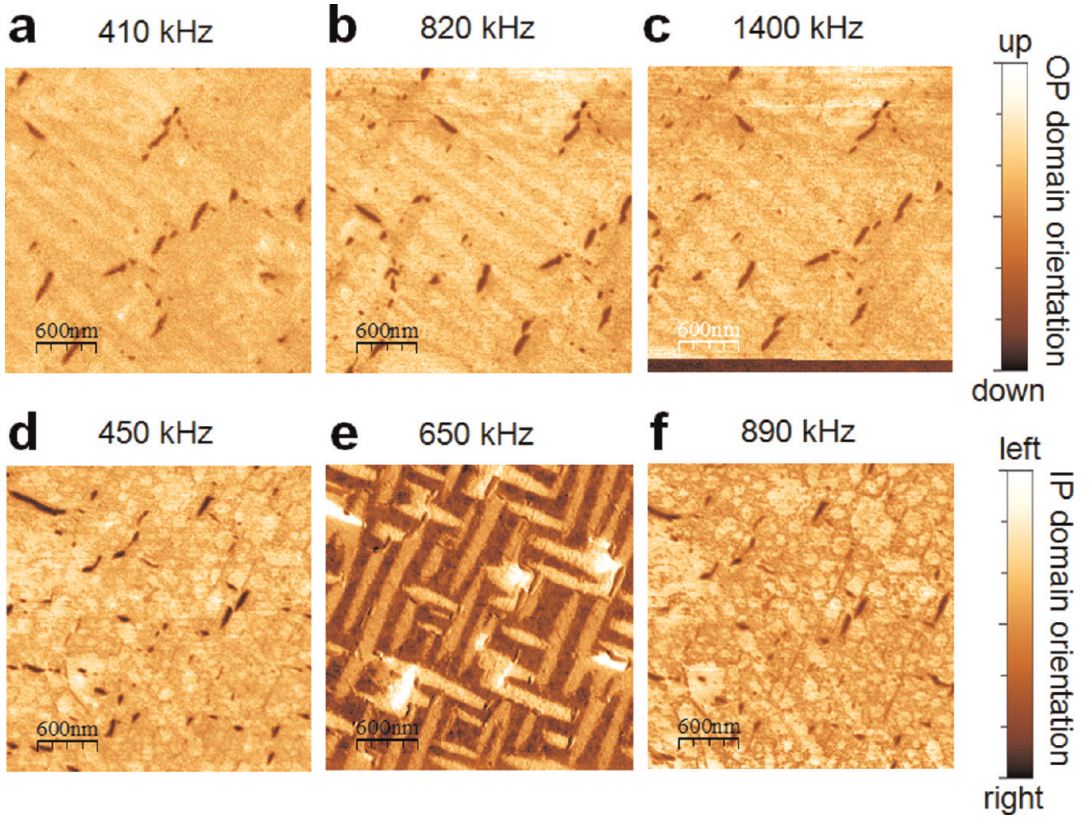

Figure 2. Single-frequency PFM images in DW. OP domain orientation with respect to the cantilever axis measured around (a) 410 kHz, (b) 820 kHz, and (c) 1400 kHz. IP domain orientation with respect to the cantilever axis measured around (d) 450 kHz, (e) 650 kHz, and (f) 890 kHz.

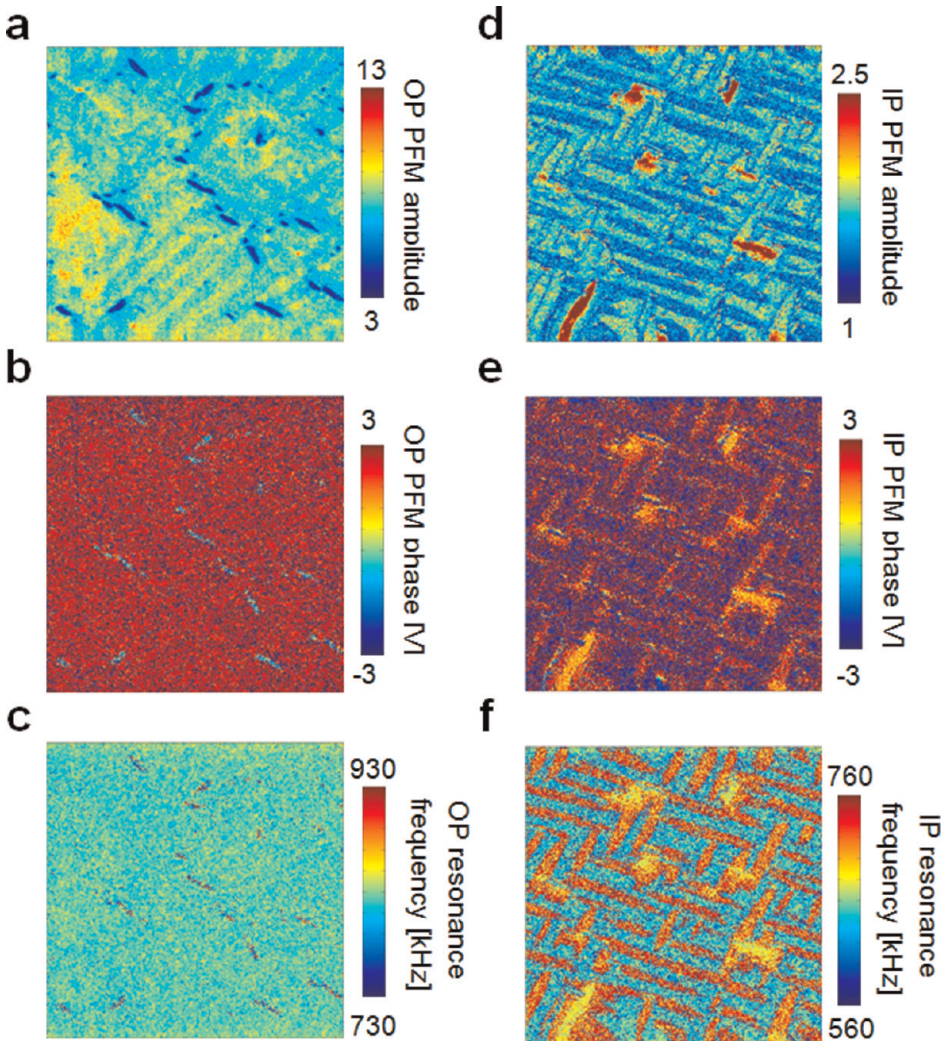

Figure 3. BE PFM images in DW. PFM amplitude, phase, and resonance frequency for OP (a–c) and IP (d–f), respectively.

methods were used for PFM imaging and switching.[38] The measurements were performed in a liquid cell with distilled water (DW) with a resistance of 18.2 MΩ/cm (Milli-Q gradient A10) as liquid medium. The cantilever dynamics with the tip in contact with the sample surface in air and DW were measured by sequentially sweeping the sample excitation bias between 0 and 2 MHz and recording the out-of-plane and in-plane surface oscillation which forms the PFM amplitude (Figure 1).

In air, the OP PFM signal shows three major contact resonance peaks. Typically, the first one around 320 kHz is used for OP PFM domain imaging, but the other resonances can be used, as well. If compared with the IP contact resonances, there are five peaks, three of them are at the same frequencies as OP and, therefore, can be identified as cross-talk between the flexural and torsional cantilever modes. However, the two peaks at 600 kHz and 1.1 MHz are pure torsional modes and, hence, can be used to image the IP domain structure.

Upon immersion in liquid, the contact resonance spectrum changes dramatically. The peak amplitudes drop, resonance peaks become much wider,

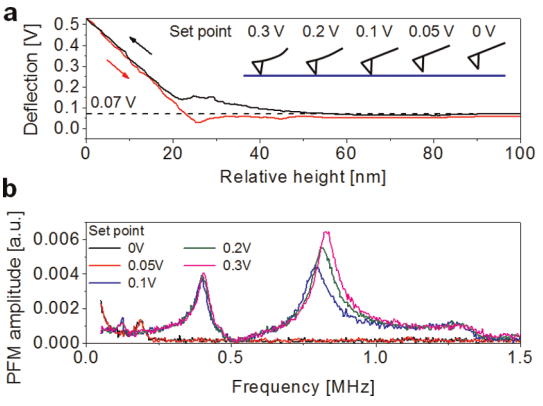

Figure 4. (a) Force–distance curve. The inlet shows the tip–sample interaction for five selected set point values between 0 and 0.3 V. (b) PFM amplitude as function of frequency of applied 1 V_{ac} voltage for set points between 0 and 0.3 V.

and resonance frequencies shift appreciably. If OP and IP contact resonance peaks are compared, three can be identified as eigenmodes for flexural oscillations and can be used to image the OP domains. However, only

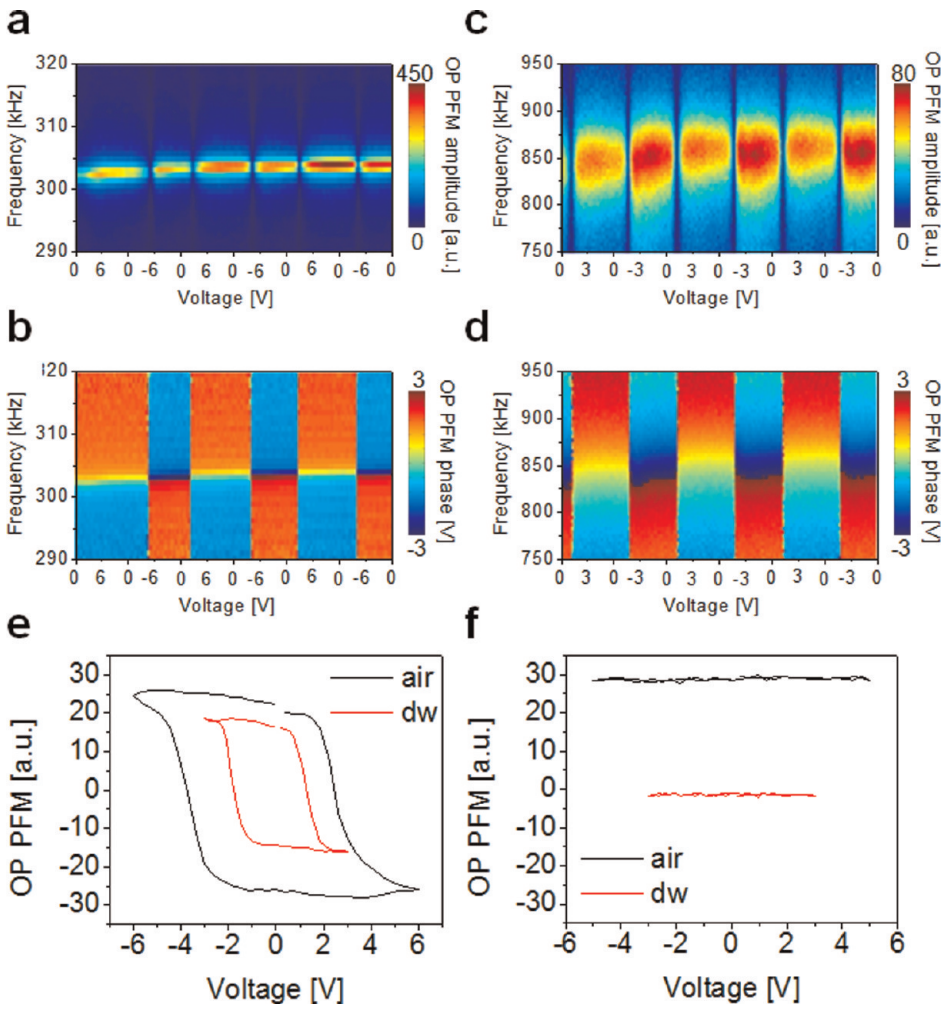

Figure 5. BE PFM voltage spectroscopy to measure piezoelectric hysteresis loops. Shown data are averaged over 100 spatial locations. (a) Two-dimensional spectrogram of OP PFM amplitude resonance peak in air as a function of voltage for three voltage sweeps between 6 and −6 V and (b) corresponding OP PFM phase. (c) Two-dimensional spectrogram of OP PFM amplitude resonance peak in DW as a function of voltage for three voltage sweeps between 6 and −6 V, and (d) corresponding OP PFM phase. (e) Piezoelectric switching loops of BFO in air and DW. (f) Piezoelectric switching loops of glass in air and DW.

one peak is now identifiable as a pure torsional mode and suitable for imaging IP domains (around 700 kHz). This attribution of the single-frequency OP and IP PFM images is demonstrated in Figure 2. The OP PFM images show a uniform contrast, whereas the IP domain structure shows the typical stripe pattern as previously reported for this material.[36,39] This shows that the polarization and piezoelectric properties are maintained under the change of the measurement environment, consistent with the findings of Rodriguez *et al.*[27] and Ferris *et al.*[25] Note that the exact resonance frequencies change slightly for different tips, typically ±30 kHz, and can also change during scanning due to tip changes.

Single-frequency measurements are subject to topography cross-talk due to position-dependent shifts in the contact resonance frequency, especially if the measurement frequency is close to a contact resonance peak.[33] To exclude the effect of the resonance peak shift, BE PFM imaging was performed in DW. During BE, the tip is simultaneously excited with multiple frequencies around the contact resonance frequency. Through Fourier transformations of the sample and cantilever response, the full contact resonance peak can be extracted. For OP and IP PFM signals, the resonance peaks around 820 and 650 kHz were used, respectively. The PFM amplitude was extracted by averaging the contact resonance amplitude peak, and the phase and resonance frequency were determined through the amplitude maximum. The extracted quantities for OP and IP PFM are shown in Figure 3.

The OP and IP PFM phase and amplitude show the same characteristics as the single-frequency images. Surprisingly, the IP resonance frequency (Figure 3f) shifts quite strongly compared to the OP resonance peak (Figure 3c). This behavior is specific to liquid and was not observed for measurements in ambient environment. This shows that imaging in liquid strongly affects the torsional cantilever dynamics and that

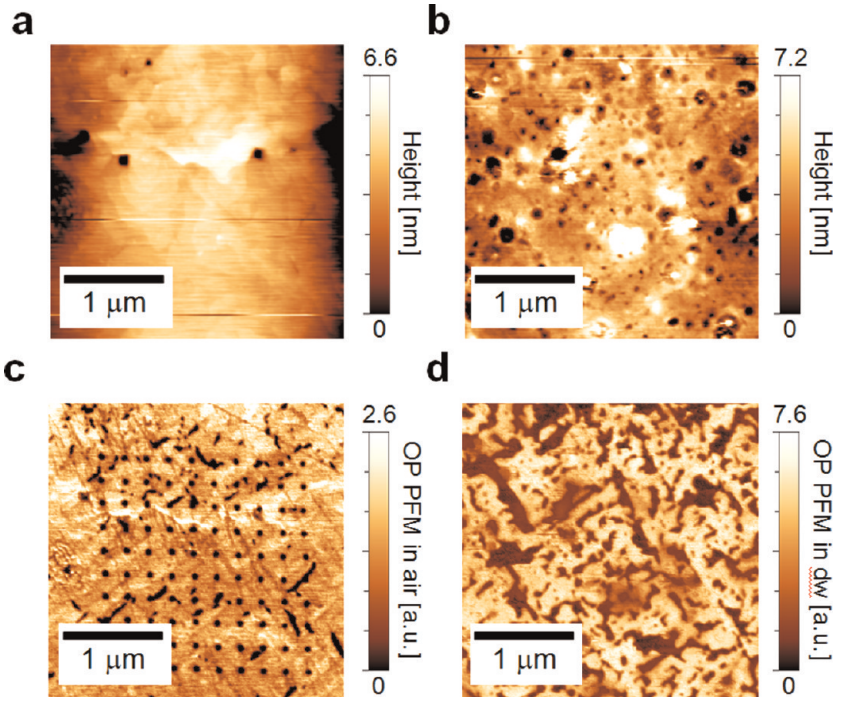

Figure 6. Topography after measuring piezoelectric hysteresis loops in (a) air and (b) DW. Single-frequency OP PFM images after measuring piezoelectric hysteresis loops in (c) air and (d) DW.

multifrequency imaging techniques are essential to reduce imaging artifacts.

In order to estimate the penetration depth of the applied ac field through the liquid and to test the influence of the water in the tip−sample contact area on the measurements, the OP PFM resonance peak is measured as a function of contact set point. The contact set point in the previous measurements was chosen to be 1 V, which corresponds to approximately 100 nN contact force between tip and sample. Force−distance curves are used to determine the set point at point of contact, as shown in Figure 4a. For large tip heights, the deflection value was 0.07 V. When the tip height is reduced, the deflection starts to increase until the linear regime of the force−distance curve is reached. When the tip is retracted again, the deflection is reduced to its baseline value again. On this basis, five different deflection values were chosen to create different contact properties between tip and sample. The idea is that the higher the contact force, the more water is displaced between the tip and the sample. The deflection set points were chosen to be 0, 0.05, 0.1, 0.2, and 0.3 V. For the first two, the tip is not in contact with the sample (<0.07 V); 0.1 V results in an intermittent contact between tip and sample, and the latter two result in a stable contact between tip and sample with different contact forces. At each set point, OP PFM frequency sweeps as in Figure 1b were performed between 0 and 1.5 MHz (Figure 4b).

It can be seen that the OP PFM signal can only be detected when the tip touches the sample surface for deflection values higher than 0.07 V; that is, the penetration of V_{ac} through the liquid can be neglected. With increasing contact force, the second resonance peak at 800 kHz shifts slighlty to higher frequencies and increases in amplitude. For set points higher than 0.3 V, the resonance peaks are not changing any more, which means at this point all of the water in the tip−sample contact area is displaced. Therefore, contact forces larger than 30 nN are required to create a stable electrical contact.

The effects of dc electrical fields on ferroelectric domains in liquid are tested by performing hysteresis loop measurements as described elsewhere.[38] A total of 100 loops were measured over a 10 × 10 grid in an area of 2 × 2 μm^2. The probing voltages were 1 V_{ac} and 6 V_{dc} for air and 3 V_{dc} for DW. The switching voltage for DW was lowered compared to that for air due to the fact that for voltages higher than 4 V_{dc}, bubble formation (*i.e.*, water splitting) was observed. Figure 5 shows the averaged switching spectrograms (OP PFM amplitude and phase as function of frequency and voltage) and extracted piezoelectric hysteresis loops for air and DW. For air, the contact resonance peak is sharp and the contact resonance frequency is constant during polarization switching (Figure 5a,b). The extracted hysteresis loop shows switching voltages of around −4 and 3 V (Figure 5e). When the spectrograms measured in air are compared to DW, it can be seen that the characteristics in the spectrograms remain, and only the width of the resonance peaks increases as seen in Figure 1b. The extracted hysteresis loop measured in DW is smaller in amplitude and switching voltages. To ensure that the signal origin comes from the sample

and is not an artifact of the experimental setup, the hysteresis loop measurements were repeated on glass as reference. In air, a strong resonance peak can be measured. However, this signal does not change with bias (Figure 5f). In DW, no signal could be detected or induced by bias. This shows that the signal measured on BFO is not due to capacitive cross-talk when an electric field is applied in a liquid medium.

To explore the domain dynamics and changes in the system induced by hysteresis loop measurements further, single-frequency OP PFM images were taken after the hysteresis measurement. In Figure 6a,c, the topography and OP PFM images after switching 10 × 10 points in air are shown, respectively. After switching, no topo changes were observed and the 10 × 10 grid of switched nanodomains can be identified; that is, polarization switching happened locally under the tip. In DW, the topography changes (Figure 6b) and domain switching well outside the switched area (Figure 6d) were observed, showing a global switching scenario. The change from local to global switching when the environment changes from air to liquid was demonstrated before by Rodriguez *et al.*[26] The topography changes occurring in DW suggest that electrochemical reactions take place during the application of switching voltages which can lead to a change in piezoresponse signal, as well.[40] Therefore, we assume that the observed differences in the hysteresis loops in air and DW are a result of global switching events instead of local plus electrochemical contributions.

CONCLUSION

To summarize, we have explored electromechanical processes in a liquid environment using voltage-modulated SPM. The cantilever contact dynamics for flexural and torsional modes is explored, providing insight into optimal conditions for in-plane and out-of-plane electromechanical imaging. We demonstrated the effect of liquid environment on sample responses to ac and dc voltages and showed that the ac sample response is barley affected by the changing environment. Future studies will inlcude the investigation of liquids of different conductivities to determine the boundary conditions to perform measurements of electromechanical phenomena in liquid. Understanding electromechanical coupling in liquid is important not only for ferroelectric oxides but also for biological and electrochemical sample systems. Here, liquid is the natural environment to maintain sample stability and functionality and the electromechanical characterization in liquid is essential in characterize these systems.

MATERIALS AND METHODS

The experiments were performed on 50 nm thin (001)-oriented multiferroic $BiFeO_3$ (BFO) films with $SrRuO_3$ (SRO) bottom electrode epitaxially grown on low miscut (<0.01°) (001) $SrTiO_3$ (STO) single-crystal substrate by pulsed laser deposition as described elsewhere.[36] PFM imaging and domain switching was performed on a commercial SPM system (MFP-3D, Asylum Research) with metal-coated SPM tips (Nanosensor). Single-frequency PFM on resonance[37] and the BE[31] method were used. For imaging, ac voltages of 1 V_{ac} were applied. For switching, we apply short (2 ms) voltage pulses with increasing and decreasing amplitude V_{dc} and probe the domains underneath the SPM tip by measuring BE PFM after each pulse in the bias-off ($V_{dc} = 0$) state to eliminate electrostatic signal contribution (voltage spectroscopy).[38] The measurements were performed in a liquid cell which provided the possibility to electrically connect to the bottom electrode (Asylum Research). As liquid environment, we used distilled water (DW) with a resistance of 18.2 MΩ/cm (Milli-Q gradient A10) in the form of a droplet on the sample surface and tip to avoid electrical shorting between the tip and the sample ground, that is, the bottom electrode of the sample.

Conflict of Interest: The authors declare no competing financial interest.

Acknowledgment. Research supported by the U.S. Department of Energy, Basic Energy Sciences, Materials Sciences and Engineering Division through the Office of Science Early Career Research Program (N.B.) and as part of the Center for Nanophase Materials Sciences, which is sponsored at Oak Ridge National Laboratory by the Scientific User Facilities Division, Office of Basic Energy Sciences, U.S. Department of Energy (S.J, S.V.K.). The work in National Chiao Tung University is supported by the National Science Council under contract no. NSC-100-2119-M-009-003.

REFERENCES AND NOTES

1. Cross, L. E. Ferroelectric Materials for Electromechanical Transducer Applications. *Mater. Chem. Phys.* **1996**, *43*, 108–115.
2. Park, S. E.; Shrout, T. R. Ultrahigh Strain and Piezoelectric Behavior in Relaxor Based Ferroelectric Single Crystals. *J. Appl. Phys.* **1997**, *82*, 1804–1811.
3. Nazri, G. A.; Pistoia, G., Eds. *Lithium Batteries: Science and Technology*; Springer Verlag: New York, 2009.
4. Adler, S. B. Factors Governing Oxygen Reduction in Solid Oxide Fuel Cell Cathodes. *Chem. Rev.* **2004**, *104*, 4791–4843.
5. Hantel, M. M.; Presser, V.; Kotz, R.; Gogotsi, Y. *In Situ* Electrochemical Dilatometry of Carbide-Derived Carbons. *Electrochem. Commun.* **2011**, *13*, 1221–1224.
6. Kepler, R. G.; Anderson, R. A. Ferroelectric Polymers. *Adv. Phys.* **1992**, *41*, 1–57.
7. Purvis, C. K.; Taylor, P. L. Piezoelectric and Pyroelectric Coefficients for Ferroelectric-Crystals with Polarizable Molecules. *Phys Rev. B* **1982**, *26*, 4564–4570.
8. Kalinin, S. V.; Rodriguez, B. J.; Jesse, S.; Karapetian, E.; Mirman, B.; Eliseev, E. A.; Morozovska, A. N. Nanoscale Electromechanics of Ferroelectric and Biological Systems: A New Dimension in Scanning Probe Microscopy. *Annu. Rev. Mater. Res.* **2007**, *37*, 189–238.
9. Scott, J. F.; De Araujo, C. A. P. Ferroelectric Memories. *Science* **1989**, *246*, 1400–1405.
10. Polla, D. L.; Francis, L. F. Processing and Characterization of Piezoelectric Materials and Integration into Microelectromechanical Systems. *Annu. Rev. Mater. Sci.* **1998**, *28*, 563–597.
11. Gruverman, A.; Auciello, O.; Tokumoto, H. Scanning Force Microscopy for the Study of Domain Structure in Ferroelectric Thin Films. *J. Vac. Sci. Technol., B* **1996**, *14*, 602–605.
12. Harnagea, C.; Pignolet, A.; Alexe, M.; Satyalakshmi, K. M.; Hesse, D.; Gosele, U. Nanoscale Switching and Domain Structure of Ferroelectric $BaBi_4Ti_4O_{15}$ Thin Films. *Jpn. J. Appl. Phys., Part 2* **1999**, *38*, L1255–L1257.

13. Kalinin, S. V.; Bonnell, D. A. Imaging Mechanism of Piezoresponse Force Microscopy of Ferroelectric Surfaces. *Phys. Rev. B* **2002**, *65*, 125408.
14. Nath, R.; Chu, Y. H.; Polomoff, N. A.; Ramesh, R.; Huey, B. D. High Speed Piezoresponse Force Microscopy: <1 Frame Per Second Nanoscale Imaging. *Appl. Phys. Lett.* **2008**, *93*, 072905.
15. Shvartsman, V. V.; Kholkin, A. L. Domain Structure of 0.8Pb(Mg1/3Bb2/3)O3−0.2PbTiO3 Studied by Piezoresponse Force Microscopy. *Phys. Rev. B* **2004**, *69*, 014102.
16. Ganpule, C. S.; Nagarajan, V.; Hill, B. K.; Roytburd, A. L.; Williams, E. D.; Ramesh, R.; Alpay, S. P.; Roelofs, A.; Waser, R.; Eng, L. M. Imaging Three-Dimensional Polarization in Epitaxial Polydomain Ferroelectric Thin Films. *J. Appl. Phys.* **2002**, *91*, 1477–1481.
17. Guyonnet, J.; Bea, H.; Guy, F.; Gariglio, S.; Fusil, S.; Bouzehouane, K.; Triscone, J. M.; Paruch, P. Shear Effects in Lateral Piezoresponse Force Microscopy at 180 Degrees Ferroelectric Domain Walls. *Appl. Phys. Lett.* **2009**, *95*, 132902.
18. Jungk, T.; Hoffmann, A.; Soergel, E. Quantitative Analysis of Ferroelectric Domain Imaging with Piezoresponse Force Microscopy. *Appl. Phys. Lett.* **2006**, *89*, 163507.
19. Roelofs, A.; Bottger, U.; Waser, R.; Schlaphof, F.; Trogisch, S.; Eng, L. M. Differentiating 180 Degrees and 90 Degrees Switching of Ferroelectric Domains with Three-Dimensional Piezoresponse Force Microscopy. *Appl. Phys. Lett.* **2000**, *77*, 3444–3446.
20. Kalinin, S. V.; Rodriguez, B. J.; Jesse, S.; Thundat, T.; Gruverman, A. Electromechanical Imaging of Biological Systems with Sub-10 nm Resolution. *Appl. Phys. Lett.* **2005**, *87*, 053901.
21. Kalinin, S. V.; Eliseev, E. A.; Morozovska, A. N. Materials Contrast in Piezoresponse Force Microscopy. *Appl. Phys. Lett.* **2006**, *88*, 232904.
22. Amatucci, G. G.; Tarascon, J. M.; Klein, L. C. CoO_2, the End Member of the Li*x*CoO_2 Solid Solution. *J. Electrochem. Soc.* **1996**, *143*, 1114–1123.
23. Balke, N.; Jesse, S.; Kim, Y.; Adamczyk, L.; Tselev, A.; Ivanov, I. N.; Dudney, N. J.; Kalinin, S. V. Real Space Mapping of Li-Ion Transport in Amorphous Si Anodes with Nanometer Resolution. *Nano Lett.* **2010**, *10*, 3420–3425.
24. Balke, N.; Jesse, S.; Morozovska, A. N.; Eliseev, E.; Chung, D. W.; Kim, Y.; Adamczyk, L.; Garcia, R. E.; Dudney, N.; Kalinin, S. V. Nanoscale Mapping of Ion Diffusion in a Lithium-Ion Battery Cathode. *Nat. Nanotechnol.* **2010**, *5*, 749–754.
25. Ferris, R.; Yellen, B.; Zauscher, S. Ferroelectric Thin Films in Fluidic Environments: A New Interface for Sensing and Manipulation of Matter. *Small* **2012**, *8*, 28–35.
26. Rodriguez, B. J.; Jesse, S.; Baddorf, A. P.; Kim, S. H.; Kalinin, S. V. Controlling Polarization Dynamics in a Liquid Environment: From Localized to Macroscopic Switching in Ferroelectrics. *Phys. Rev. Lett.* **2007**, *98*, 247603.
27. Rodriguez, B. J.; Jesse, S.; Baddorf, A. P.; Kalinin, S. V. High Resolution Electromechanical Imaging of Ferroelectric Materials in a Liquid Environment by Piezoresponse Force Microscopy. *Phys. Rev. Lett.* **2006**, *96*, 237602.
28. Rodriguez, B. J.; Jesse, S.; Habelitz, S.; Proksch, R.; Kalinin, S. V. Intermittent Contact Mode Piezoresponse Force Microscopy in a Liquid Environment. *Nanotechnology* **2009**, *20*, 195701.
29. Noh, J. H.; Nikiforov, M.; Kalinin, S. V.; Vertegel, A. A.; Rack, P. D. Nanofabrication of Insulated Scanning Probes for Electromechanical Imaging in Liquid Solutions. *Nanotechnology* **2010**, *21*, 365302.
30. Rodriguez, B. J.; Callahan, C.; Kalinin, S. V.; Proksch, R. Dual-Frequency Resonance-Tracking Atomic Force Microscopy. *Nanotechnology* **2007**, *18*, 475504.
31. Jesse, S.; Kalinin, S. V.; Proksch, R.; Baddorf, A. P.; Rodriguez, B. J. The Band Excitation Method in Scanning Probe Microscopy for Rapid Mapping of Energy Dissipation on the Nanoscale. *Nanotechnology* **2007**, *18*, 435503.
32. Proksch, R.; Kalinin, S. V. Energy Dissipation Measurements in Frequency-Modulated Scanning Probe Microscopy. *Nanotechnology* **2010**, *21*, 455705.
33. Jesse, S.; Guo, S.; Kumar, A.; Rodriguez, B. J.; Proksch, R.; Kalinin, S. V. Resolution Theory, and Static and Frequency-Dependent Cross-Talk in Piezoresponse Force Microscopy. *Nanotechnology* **2010**, *21*, 405703.
34. Kiracofe, D.; Raman, A. Quantitative Force and Dissipation Measurements in Liquids Using Piezo-Excited Atomic Force Microscopy: A Unifying Theory. *Nanotechnology* **2011**, *22*, 485502.
35. Mirman, B.; Kalinin, S. V. Resonance Frequency Analysis for Surface-Coupled Atomic Force Microscopy Cantilever in Ambient and Liquid Environments. *Appl. Phys. Lett.* **2008**, *92*, 083102.
36. Balke, N.; Choudhury, S.; Jesse, S.; Huijben, M.; Chu, Y. H.; Baddorf, A. P.; Chen, L. Q.; Ramesh, R.; Kalinin, S. V. Deterministic Control of Ferroelastic Switching in Multiferroic Materials. *Nat. Nanotechnol* **2009**, *4*, 868–875.
37. Harnagea, C.; Alexe, M.; Hesse, D.; Pignolet, A. Contact Resonances in Voltage-Modulated Force Microscopy. *Appl. Phys. Lett.* **2003**, *83*, 338–340.
38. Jesse, S.; Maksymovych, P.; Kalinina, S. V. Rapid Multidimensional Data Acquisition in Scanning Probe Microscopy Applied to Local Polarization Dynamics and Voltage Dependent Contact Mechanics. *Appl. Phys. Lett.* **2008**, *93*, 112903.
39. Zavaliche, F.; Das, R. R.; Kim, D. M.; Eom, C. B.; Yang, S. Y.; Shafer, P.; Ramesh, R. Ferroelectric Domain Structure in Epitaxial $BiFeO_3$ Films. *Appl. Phys. Lett.* **2005**, *87*, 182912.
40. Kalinin, S. V.; Jesse, S.; Tselev, A.; Baddorf, A. P.; Balke, N. The Role of Electrochemical Phenomena in Scanning Probe Microscopy of Ferroelectric Thin Films. *ACS Nano* **2011**, *5*, 5683–5691.